Journal of Advanced Research 31 (2021) 155–163

Contents lists available at ScienceDirect

Journal of Advanced Research

journal homepage: www.elsevier.com/locate/jare

Application of M1 macrophage as a live vector in delivering nanoparticles for *in vivo* photothermal treatment

Nu-Ri Im [a,1], Taeseok Daniel Yang [b,c,1], Kwanjun Park [d], Jang-Hoon Lee [b], Jonghwan Lee [b], Yoon Hyuck Kim [e], Jae-Seung Lee [e], Byoungjae Kim [a,f], Kwang-Yoon Jung [a], Youngwoon Choi [c,d,g], Seung-Kuk Baek [a]

[a] Department of Otolaryngology-Head and Neck Surgery, Korea University, Seoul 02841, South Korea
[b] Department of Biomedical Engineering, Brown University, Providence, RI 02912, USA
[c] School of Biomedical Engineering, Korea University, Seoul 02841, South Korea
[d] Department of Bioengineering, Korea University, Seoul 02841, South Korea
[e] Department of Materials Science and Engineering, Korea University, Seoul 02841, South Korea
[f] Department of Neuroscience Research Institute, Korea University, Seoul 02841, South Korea
[g] Interdisciplinary Program in Precision Public Health, Korea University, Seoul 02841, South Korea

GRAPHICAL ABSTRACT

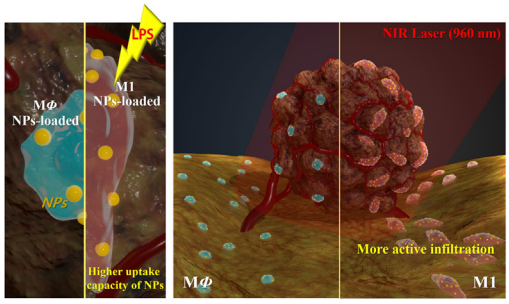

ARTICLE INFO

Article history:
Received 14 September 2020
Revised 14 January 2021
Accepted 19 January 2021
Available online 1 February 2021

Keywords:
M1 macrophage
Photothermal treatment
Photothermal effect
Live cell vector
Cancer therapy
Medical optics and biotechnology

ABSTRACT

Introduction: To enhance photothermal treatment (PTT) efficiency, a delivery method that uses cell vector for nanoparticles (NPs) delivery has drawn attention and studied widely in recent years.
Objectives: In this study, we demonstrated the feasibility of M1 activated macrophage as a live vector for delivering NPs and investigated the effect of NPs loaded M1 stimulated by Lipopolysaccharide on PTT efficiency *in vivo*.
Methods: M1 was used as a live vector for delivering NPs and further to investigate the effect of NPs loaded M1 on PTT efficiency. Non-activated macrophage (MΦ) was stimulated by lipopolysaccharide (LPS) into M1 and assessed for tumor cell phagocytic capacity towards NPs
Results: We found M1 exhibited a 20-fold higher uptake capacity of NPs per cell volume and 2.9-fold more active infiltration into the tumor site, compared with non-activated macrophage MΦ. We injected M1 cells peritumorally and observed that these cells penetrated into the tumor mass within 12 h. Then, we conducted PTT using irradiation of a near-infrared laser for 1 min at 1 W/cm^2. As a result, we confirmed that using M1 as an active live vector led to a more rapid reduction in tumor size within 1 day

Peer review under responsibility of Cairo University.
[1] These authors contributed equally to this work.
E-mail addresses: youngwoon@korea.ac.kr (Y. Choi), mdskbaek@gmail.com (S.-K. Baek)

https://doi.org/10.1016/j.jare.2021.01.010

indicating that the efficacy of PTT with NPs-loaded M1 is higher than that with NPs-loaded MΦ.
Conclusion: Our study demonstrated the potential role of M1 as a live vector for enhancing the feasibility of PTT in cancer treatment.

Introduction

Many different methods have been used for treating cancer patients in clinics, from surgical approach of direct tumor resection to targeted therapies such as chemotherapy and radiotherapy [1,2]. To enhance cancer treatment efficacy such as progression free recover and high survival rates, combined therapy with two or three of the conventional methods is often used, depending on the type and stage of cancer [3,4]. However, while combined therapy moderately increases efficacy, this strategy is accompanied by toxicity and low specificity posing a significant hindrance to effective therapy. Recent studies focusing on photothermal therapy (PTT) have shown promising results in tumor removal with reduced toxicity [5–11]. PTT induces cancer cell death in locally targeted tumor sites using heat generated from nanoparticles (NPs) in the tumor tissue after being exposed to near-infrared (NIR). Here, NIR can be penetrated non-invasively or minimally-invasively, which allows sufficient depth for a desirable optical window in biological tissues. As a photosensitizer, NPs is excited by NIR and then releases vibration energy converted to thermal energy. That NPs can be modulated by the relative core size and shell-thickness which determines the thermal efficiency and specific absorption wavelength. Therefore, the efficiency of PTT relies intensively on heat energy generated from NPs activated by irradiation of NIR light. A target-specific delivery of NPs plays a crucial role in not only generating intensive heat energy but also minimizing thermal damage of the surrounding tissues and molecular toxicity of other systemic organs such as liver and spleen, which results in high efficiency and improved safety. Therefore, it is important to improve the target specificity of NPs in delivery.

Several strategies have been employed to enhance target specificity. Tumor-specific materials such as chains of polyethylene glycol (PEG) and the epidermal growth factor receptor (EGFR) were conjugated on the surface of NPs [12,13] to improve the enhanced permeability and retention (EPR) effect for immature tumor vasculature [14,15], subsequently, increased circulation times [16] and accumulation of nanoparticles in the tumor sites. However, high concentrations of NPs were still observed in the liver and spleen, and only a small fraction of the injected dose of NPs reached the tumor site [17]. To improve this low target specificity, a different method using macrophages as a live cell vector was recently introduced [6,9–11]. Macrophages being immune cells, engulf NPs and carry them to target sites as part of immune response where they are irradiated by NIR laser. These studies demonstrated that peritoneal macrophages (non-activated) as a live vector for delivering NPs through peritumoral injections, improves the effectiveness of PTT without target specificity [9–11]. As a result, the tumor mass could be destructed by photothermal effect of NPs that were delivered by macrophages. After PTT, NPs aggregate into coarse particles which cannot diffuse to the other organs. However, since non-activated macrophages do not have specificity towards tumor cells, activated macrophages would be an excellent alternative due to their enhanced accumulation of NPs and high specificity enabling them to directly penetrate into tumor mass.

Classical-activated macrophage, M1, suppresses proliferation, reduces angiogenesis and induces the apoptosis of cancer cells [18,19]. More importantly, it responds to the signals released by the tumor microenvironment such as cytokines, chemokines, and growth factors, and directly infiltrates the tumor microenvironment. In addition, M1 has exhibited a higher phagocytic ability and a larger cell size than the non-activated macrophage, therefore, it has a potentially enhanced NPs uptake capacity and the migration capability [20,21].

In this study, we demonstrated the feasibility of M1 as a live vector for delivering NPs and investigated the effect of NPs loaded M1 on PTT efficiency. Non-activated macrophage (MΦ) was stimulated by Lipopolysaccharide (LPS) into M1 which showed a higher uptake capacity of NPs per cell with higher phagocytotic activity and more active infiltration into the tumor site due to tumor-associated activity. With M1 as an active live vector, we established the optimal NPs concentration and PTT administration time after M1 injection. Our study serves as a baseline for further enhancing the feasibility of PTT with M1 as a live vector.

Materials and methods

The animal experiments in this study were approved and confirmed by our institutional review board for animal research, the Korea University Institutional Animal Care and Use Committee (KUIACUC-2016-0214), and performed in accordance with relevant guidelines and regulations.

Preparation of gold nanoparticles

The core silica particles of gold-nanoshell (gold-NS) were synthesized following a modified Stöber method [22]. The surface of the silica particles (50 mL in aqueous solution) was amine-activated using 3 -amino propyl trimethoxy silane (APTMS, 20 μL) for 6 h. The tiny gold nanoparticles were separately synthesized by rapidly combining an aqueous $HAuCl_4$ solution (2 mL, 27 mM) with an aqueous Tetrakis hydroxymethyl phosphonium chloride (THPC) solution (47 mL, 0.02% THPC, 0.011 M NaOH). About 100 μL of the amine-functionalized silica nanoparticle solution was gently added to a 1 mL of the tiny gold nanoparticle solution and shaken for about 1 h. The silica-gold nanoparticle composite solution (20 μL) was combined with a growth solution (1.5 mL of 27 mM $HAuCl_4$ and 100 mL of 1.81 mM K_2CO_3) and 27 μL of formaldehyde to promote the gold shell growth. For more information on the preparation of the gold-NS, refer to the reference number 10.

Preparation of cancer cells and xenotransplantation

Head and neck squamous cancer cell line (SNU-1041) derived from human pharyngeal cancer was cultured in a mixture of Roswell Park Memorial Institute (RPMI) 1640 (Gibco BRL, USA) containing L-glutamine, 10% fetal bovine serum (FBS; Gibco BRL, USA) and 1% penicillin/streptomycin solution (PS; Welgene, Korea) and incubated in a 5% CO_2 incubator. For the in vitro experiments, the cancer cells (1×10^6 cells/mL) were cultured in a 35-mm culture dish and maintained in a 5% CO_2 incubator at 37 °C for 3 days. For the xenotransplantation, the cancer cells were prepared to 1×10^6 cells/mL, then injected subcutaneously into the flanks of nude mice (BALB/c-nu/nu, female, aged 6 weeks) using an insulin syringe [10]. Body weights of the mice and growing tumor size were monitored and measured three times per week. Then PTT was performed when the diameter of the tumor became greater than 10 mm.

Activation of M1 macrophage and qPCR analysis

The murine macrophage cell line RAW 264.7 was obtained from the Korean cell line bank. The cells were cultured in Dulbecco's Modified Eagle Medium (DMEM) solution (Welgene, Korea) contained with 10% FBS and 1% PS in a 100-mm culture dish. Cultured cells were maintained in a 5% CO_2 incubator at 37 °C, and the medium was changed every 2 days. The murine macrophage cell line RAW 264.7 cells were seeded in culture dishes for 24 h and then incubated at 37 °C, 5% CO2 with 100 ng/mL LPS (PeproTech, Korea) for 24 h. These cells were analyzed by a quantitative real-time polymerase chain reaction (qPCR). Gene expression in the epithelial cell was measured by qPCR. Total RNA was extracted from approximately 5 × 105 cells using TRIzol (Qiazen, USA) and RNase-free DNase I (Qiagen, USA). The 1 ug RNA were reverse transcribed to cDNA using amfiRivert cDNA synthesis platinum master mix (GenDEPOT, USA). The prepared cDNA was amplified and quantified using SYBR green master mix (Qiagen, USA) with the following primers.

To confirm activated M1 of macrophage, the gene expression in the macrophage cells was measured by qPCR. The prepared cDNA was amplified and quantified using SYBR green master mix (Qiagen, USA) with the following primers: Glyceraldehyde 3-phosphate dehydrogenase (GAPDH), forward 5′-T TGT CGT GGA GTC TAC TGG T- 3′ and reverse 5′-GA GTT GTC ATA TTT CTC GT-3′; Inducible nitric oxide synthase (iNOS), forward 5′-TT TGC TTC CAT GCT AAT GCG AAA G-3′ and reverse 5′-GC TCT GTT GAG GTC TAA AGG CTC CG-3′. The qPCR was performed using a quantitative thermal cycler system (TP800/TP860, Japan) with 40 cycles of a 2-step reaction consisting of denaturation at 95 °C for 15 s, followed by annealing/extension at 60 °C for 45 s. Data were analyzed using the $\triangle Ct$ method.

Flow cytometry (FACS) analysis

After LPS stimulation, cells were scraped and resuspended in ice-cold PBS containing 5% bovine serum albumin (BSA). For the flow cytometry, cells were stained using intracellular staining protocol with fixation/permeabilization buffer solution (BD Biosciences, USA) for 30 min at 4 °C, then incubated with 0.06 μg/mL of iNOS-PE antibody (Invitrogen, USA) in the darkroom for 30 min before sorting. FACS analysis was performed using FACS Canto II (BD Biosciences, USA) then MΦ and M1 were defined and collected F4/80-positive and iNOS-positive cells.

Preparation of gold nanoparticles loaded macrophages

The NPs of 3 pM and suspended M1 of 2×10^4 cells/mL were co-incubated and gently shaken on the orbital shaker for 2 h [10]. Then approximately 1×10^4 cells/mL of NPs-loaded M1 was used. The mixture containing the NPs and macrophages were seeded onto a 35 mm^2 cell culture dish and incubated for 2 h to allow the cells to settle down and adhere to the bottom of the dish. We then collected using a cell scraper, and made the cell suspension with 1×10^4 cells/mL. Finally, approximately 1×10^4 cells/mL of NPs-loaded macrophages were used.

Quantitative phase microscopy

The quantitative phase imaging (QPI) system was based on a synthetic aperture microscope employing Mach-Zehnder interferometry [23,24]. A He-Ne laser with a wavelength of 632.8 nm was used as a light source. The cells were prepared between two slide glasses and then placed on a live cell chamber for observation. For high-resolution and high-speed imaging, a high numerical aperture (NA) objective lens (100×, 1.4 NA, oil immersion) and a 2-D Galvanometer scanning mirrors were used. The 200 interferograms were acquired at 150 frames per second while varying the illumination angle from 0 to 1.4 NA, one at a time. All the images were converted into complex field maps using the Fast Fourier Transformation (FFT) method and then synthesized in an extended single aperture to enhance the spatial resolution and the image quality [22]. With this method, the phase information of samples was obtained with a spatial resolution of 276 nm and an improved signal-to-noise ratio.

In vivo bioluminescence measurements

To assess the movement of macrophages toward the tumor site, MΦ and M1 were transfected with the luciferase gene. RAW 264.7 cells were seeded (5×10^4 cells/well) into 12-well flat bottom culture plates and incubated in a 5% CO_2, at 37 °C. When the cells reached about 70% confluence of the well, the gene transfection was performed by adding 1 μg vector of pGL4.51[luc2/CMV/Neo] (Promega, USA), lipofectamine 2000 (Thermo Fisher Scientific, USA) reagent 5 μL with opti-MEM medium 50 μL (Gibco, USA), and the cells were placed in an incubator for 48 h in 5% CO_2 at 37 °C. Then the medium was replaced with fresh DMEM medium containing 10% FBS, 1% P/S, and 1% L-glutamine. Immediately, neomycin antibiotics (500 μg/ml, Sigma Aldrich, USA) added for the selecting the transfected cells and then incubated for 48 h in a 5% CO_2, at 37 °C. Luciferase activity was measured using a multi plate reader Envision XCITE (PerkinElmer Life & Analytical Sciences, USA). Transfected cells were injected into four locations around the xenograft tumor mass. To image the transfected cell, a PBS buffer with 100 μL of 15 mg/ml D-luciferin (Promega, USA) was injected subcutaneously 30 min before imaging. For evaluating of cell penetration in the tumor site, *in vivo* bioluminescence imaging was carried out using NightOWL II LB 983 (Berthold Technologies, Germany) every 12 h for 72 h and analyzed by photometry software, indiGO™ (Ver. 2.0.5.0).

Immunofluorescence analysis

For the immunofluorescent study, the mice were sacrificed 12 h after macrophages injection, and the tumor tissues were dissected and fixed by 4% paraformaldehyde. To permeabilize the membranes, the frozen sections (10 μm) of tumor tissues were cut and treated with 0.3% Triton X-100 in PBS for 10 min. After washing in PBS, the tissue sections were incubated overnight at 4 °C with F4/80 antibody (1:100, Abcam, UK) or iNOS antibody (1:50, Invitrogen, USA) for 24 h, then treated with secondary antibodies Alexa Fluor® 488 goat anti-rabbit (Abcam, USA) or Alexa Fluor® 594 goat anti-rat (Abcam, USA) for 2 h. And 4′,6-diamidino-2-phenylindole (DAPI; Sigma-Aldrich, USA) at a concentration of 0.1 μg/mL in PBS was used to counterstain nuclei. F4/80, iNOS, and DAPI were represented as red, green, and blue colors, respectively. The fluorescent cell images were captured with a Slide scanner Axio Scan Z1 (ZEISS, Germany).

Statistical analysis

The statistical results are denoted as mean value ± standard deviation (SD) measured after each experiment (N). The data were based on one-way analysis of variance (ANOVA) and the *p*-value of<0.05 was considered statistically significant.

Results

Evaluation of M1 activated macrophages and uptake capacity of NPs

The murine macrophage RAW 264.7 cell line was activated into M1 by LPS (see Material and Methods). To confirm M1 activation, we analyzed the mRNA expression with iNOS, a known classical marker of M1, using qPCR as shown in Fig. 1(a). iNOS expression ratio of LPS (100 ng/mL) was 13.99 ± 0.21 ($p < 0.05$) that is about 14-fold higher than normal control MΦ (N = 4). To select M1 cells, we used FACS as shown in Fig. 1(b). We set the gate with an unstimulated level at 1.7% and the LPS stimulated M1 collected was 14% out of the whole population.

In addition, macrophages showed morphological differences between MΦ and M1 polarized [25,26] when cells were observed by QPI in 3-D as shown in Fig. 1(c). MΦ appeared as small and round-shaped with an average size of 15.45 ± 1.23 μm in diameter (N = 5). M1 appeared as large and heterogeneous bipolar shaped characterized by an elongated cell body with a cytoplasmic extension with an average length of 38.71 ± 7.39 μm (N = 5). Sphericity for MΦ and M1 were measured as 0.187 ± 0.004 and 0.077 ± 0.003 ($p < 0.001$), respectively (see Table 1). Importantly, NPs volume per cell (VPC) indicating the uptake capacity was clearly distinguished from QPI images between the two macrophage groups. From the phase images of the cells uptaking the NPs, the phase contribution only by the NPs can be separated with the morphology of a living cell. This is because the NPs show peculiarly high phase values compared to the remaining cellular regions. The separated phase values of NPs are converted into a thickness map, then the total volume of NPs is determined by selectively integrating the thickness map with respect to the NPs. MΦ was 0.25 ± 0.09, whereas M1was 5.11 ± 2.73 ($p < 0.01$), 20-fold significantly higher than MΦ [27]. Since we used 27.5 pM as the concentration of NPs from the previous study [9–11], the appropriate concentration of NPs for this study would be approximately 1.5 pM based on 20-fold higher

Table 1
Summary of the characteristic values of MΦ and M1.

N = 5	MΦ	M1	*p*-value
Sphericity	0.187 ± 0.004	0.077 ± 0.003	<0.001
Particle volume per cell [mm³/cell]	0.250 ± 0.085	5.111 ± 2.733	<0.01

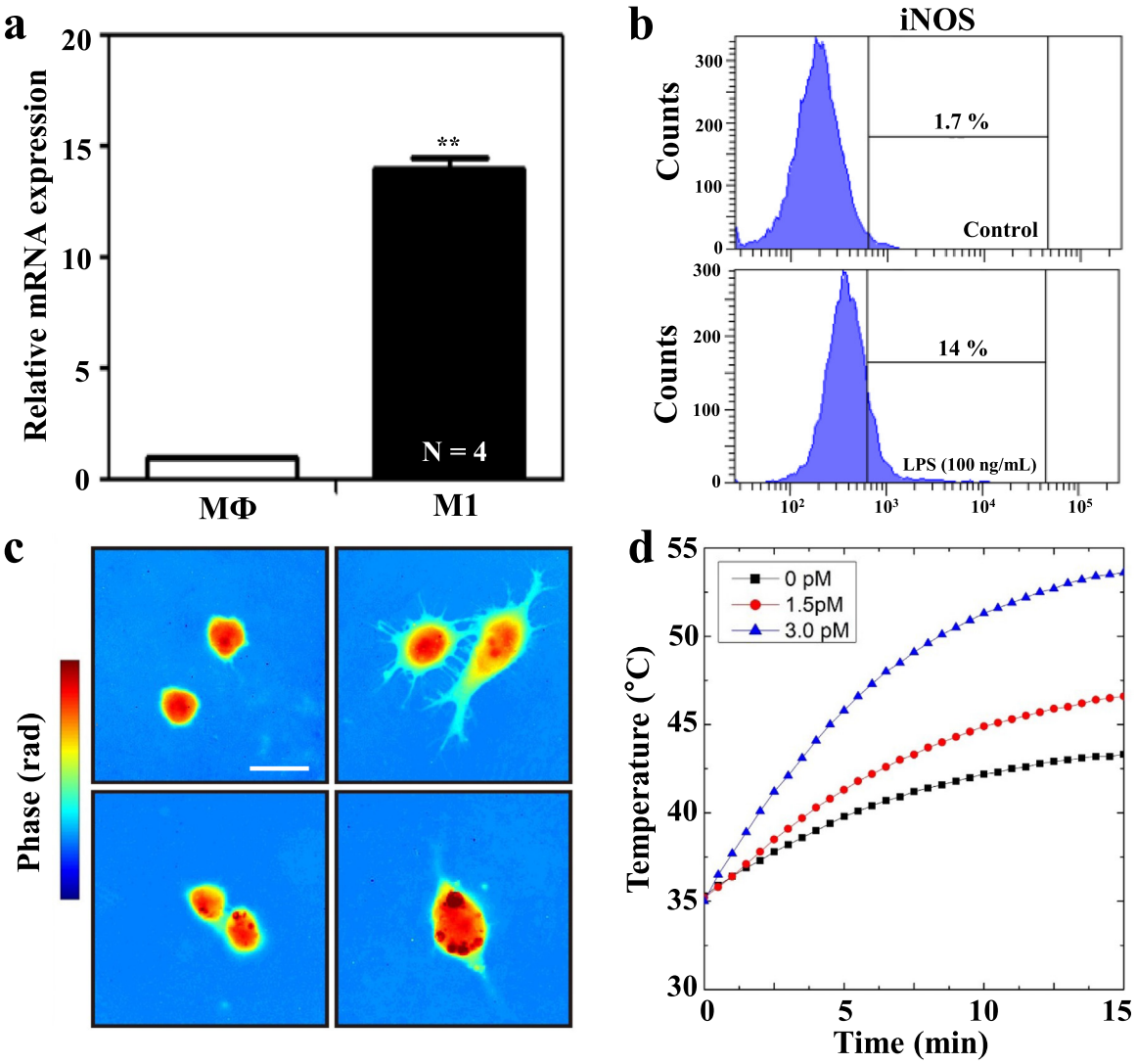

Fig. 1. LPS stimulated macrophage (M1) and uptake capacity of NPs. (a) M1 showed a 14-fold mRNA gene expression in iNOS using qPCR analysis. (b) iNOS stained M1 cells collected were 14% of the whole population using FACS. (c) MΦ and M1 imaged with QPI method showing the uptake capacity of NPs. (d) The medium temperatures were measured with changing NPs concentration, 0, 1.5 and 3.0 pM within the NPs-mixed medium. Scale bar is 20 μm.

VPC for M1 over MΦ, as shown in Table 1. To evaluate the heat efficiency of NIR irradiated NPs, we tested the NPs at a concentration of 0, 1.5, and 3.0 pM within the NPs-mixed medium.

The concentration of 1.5 pM showed a 20-fold increase in uptake capacity of NPs in M1, however, the target temperature of 44 °C with irradiation of 1 W/cm^2 for 5 min could not be achieved at 1.5 pM as shown in Fig. 1(d) red line [9]. Therefore, we set the optimal concentration of NPs at 3.0 pM of M1, which means a 2-fold increase in NPs uptake capacity compared to 27.5 pM of MΦ.

Uptake capacity of NPs and in vitro photothermal effect

We prepared two squamous cancer monolayer models with NPs-loaded MΦ and M1 (1×10^4 cells/mL) with NPs concentration of 3.0 pM. They were exposed to NIR laser at 960 nm with 1 W/cm^2 for 5 min. In the MΦ monolayer model, the cancer cell area decreased in proportion, shrank, and detached from the bottom of the culture dish (N = 5) as shown in Fig. 2(a). After PTT, the average detached area fraction for MΦ was 58.21 ± 4.96%. The average detached area fraction for M1 was higher, 65.71 ± 3.19% as shown in Fig. 2(b). Although the cellular damage rate increased slightly (1.13-fold, $p < 0.05$), this increase confirmed the relatively enhanced uptake capacity of NPs for M1, which could ultimately improve the effectiveness of PTT.

Identification of M1 macrophage actively penetrating into tumor site

To investigate the migration of both MΦ and M1 into the tumor xenograft, we traced the movement of cells transfected with the luciferase. Bioluminescence intensity was measured by a red circle every 12 h for 72 h as shown in Fig. 3(a). After peritumoral injection, the bioluminescence intensity (1×10^3) of MΦ decreased gradually from 1.41 ± 0.03 to 0.48 ± 0.02, within the 72 h. On the other hand, M1 infiltrated towards the tumor site as represented by luciferase expression intensity, and its intensity increased rapidly from 0.51 ± 0.05 to 7.12 ± 0.08 within 12 h as shown in Fig. 3(b). These results imply that M1 actively penetrated into the tumor site as a 2.9-fold because M1 macrophages were involved in tumor-associated inflammation.

To further validate the active migration of M1, we performed immunofluorescence assay with F4/80 and iNOS representative of all macrophages and M1-specific markers. Tissues were dissected into pieces of 10 μm thickness at 12 h after the subcutaneous injection of macrophages. A total of five tissues (N = 5) were stained for each group. The M1 group showed a higher intensity for both F4/80 (as a red color) and iNOS (as a green color) and bigger stained areas of macrophages than the MΦ group as shown in Fig. 3(c). Cancer and macrophage cell nuclei were stained with DAPI (as a blue color) to show cell distributions of the whole dissected tissue. And the 'Merge' showed F4/80, iNOS and DAPI merged into a single image, here, an orange color represented qualitatively the portion of M1 among all macrophages. For the quantitative comparison of cell penetration between M1 and MΦ, we calculated a normalized intensity and a stained area fraction as shown in Fig. 3(d). For F4/80, the normalized intensity values of the MΦ and the M1 groups were 48.08 ± 2.46 and 58.42 ± 8.16, respectively. The stained area fraction values were 22.48 ± 2.90 and 38.65 ± 3.68, respectively. Similarly, for iNOS, the normalized intensity and stained area fraction of the MΦ and M1 groups were 17.57 ± 2.28 and 25.75 ± 6.72, 8.54 ± 1.08 and 21.54 ± 0.79, respectively. Based on these results, M1 showed relatively fast penetration to the tumor site, implying that the NPs delivery by M1 is more efficient than that of MΦ.

In-vivo photothermal treatment effect with M1 as an active live cell vector

To examine the M1 effect on PTT, we prepared a total of 24 mice and divided them into 3 groups: control, MΦ, and M1. For the control group, we illuminated the tumor mass using a NIR laser with 1 W/cm^2 for 1 min without any injection of NPs. The tumor mass did not show change with NIR laser irradiation as shown in Fig. 4(a), the tumor volume showed a gradual increase (a black line) to 404.01 ± 71.20 mm^3 during a 4-day observation period as shown in Fig. 4(b), and the mice body weights were well preserved as shown in Fig. 4(c).

For MΦ and M1 groups (N = 8), the NPs-loaded macrophages were injected to peritumoral region subcutaneously, and PTT using a NIR laser with 1 W/cm^2 for 1 min was administered 12 h after the injection. Both groups showed a reduction in tumor volume to 13.91 ± 10.81 mm^3 and 0.52 ± 0.01 mm^3 in 4 days after the NIR laser irradiation as shown in Fig. 4(b). The M1 group showed a rapid decrease of the tumor mass (10.01 ± 6.37 mm^3) in 1 day, whereas the MΦ group showed a slow reduction (118.27 ± 45.48) in 1 day, and gradually diminished until 4 days. The MΦ group showed approximately 40.7% shrinkage of the tumor mass 1 day after PTT whereas that of the M1 group was 94.9%. After 4 days, the MΦ group and M1 group showed 93.0% and 99.7% shrinkage of

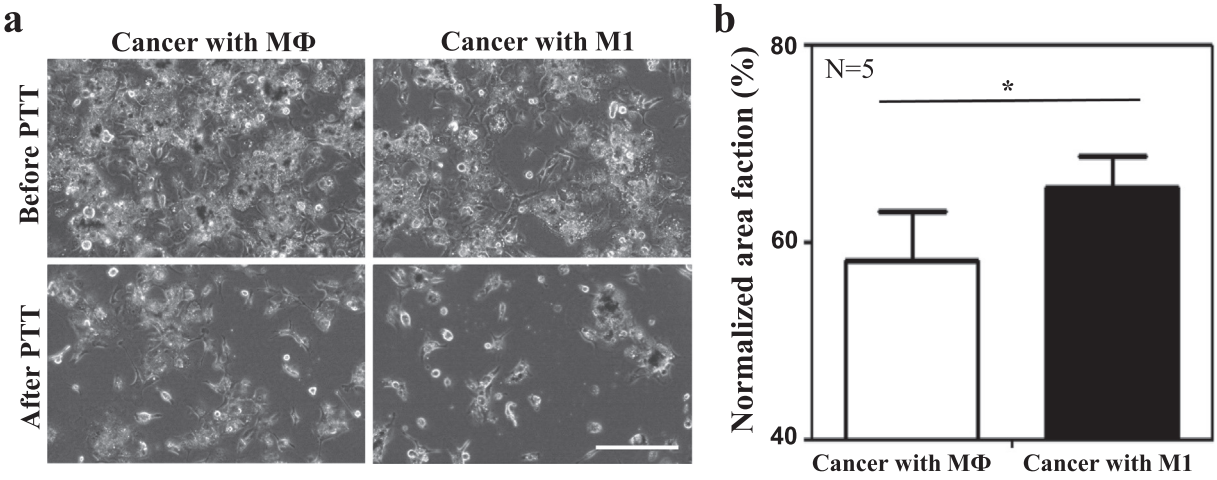

Fig. 2. *In vitro* evaluation of a heat efficiency with NPs-loaded macrophages. (a) Phase contrast image showed before and after PTT using cancer cells with NPs-loaded macrophages. (b) The histogram showed the area fraction after PTT. Scale bar is 500 μm.

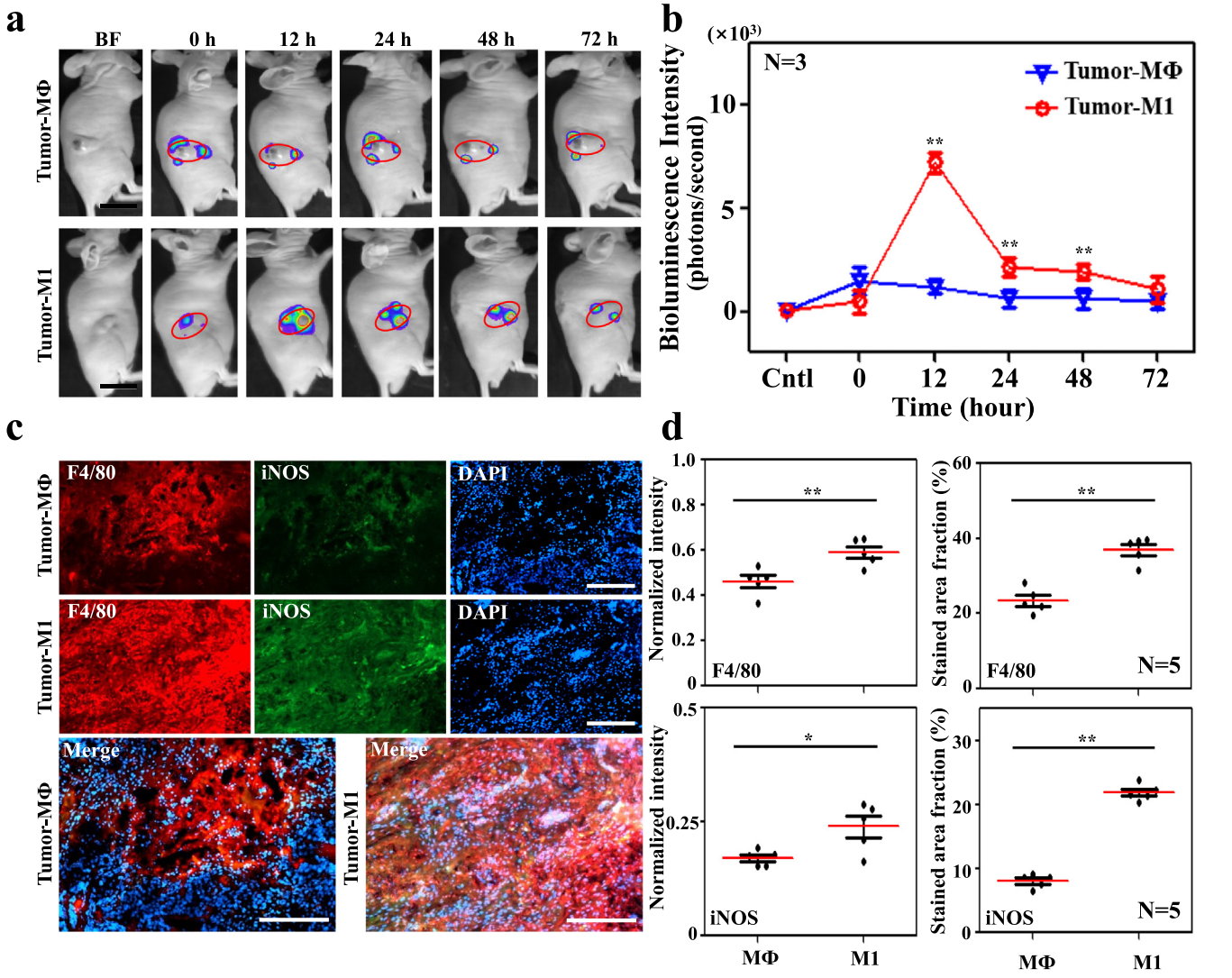

Fig. 3. The evaluation of macrophage penetration into the tumor mass. (a) The bioluminescence intensity showed the penetration of MΦ and M1 into the tumor mass (in the red circle) for 72 h. Scale bar is 2 cm. (b) The graph represented the bioluminescence intensity for 72 h. (c) The images of multi-stained immunofluorescence assay with F4/80, iNOS, and DPI showed in the tumor tissue sections at 12 h. Scale bar is 200 μm. (d) The intensity and stained area fraction measured by the immunofluorescence assay.

the tumor mass. There was no significant difference in body weight was between groups M*Φ* and M1 groups, and the control group. Further, in the M1 group, we observed indurated tissues with a crust caused by heat damage after PTT treatment which healed 2 weeks after PTT. This implied that PTT using NPs loaded with M1 is more efficient than with M*Φ*.

For immunohistology (H&E) assay, the mice were sacrificed, and the tumor mass was dissected 4 days after PTT. The control group showed densely grown cancer cells. In the M*Φ* and M1 groups, extensive cellular destructions were observed within the stained tissue sections. The tissue sections for M1 had only fibrotic tissues present without any tumor cell, whereas cancer cells were still present in the tissue sections of M*Φ* as shown in Fig. 4(d). These results confirm that the efficiency of PTT positively correlates with the rate of active penetration of M*Φ* and M1 into the tumor site as shown in Fig. 3.

Discussion

The delivery method of NPs to the target region is considered as one of the key factors affecting therapy efficiency. Since the delivery method determines the density of NPs in the target region, it also affects the heat energy generated by PTT. To enhance NPs delivery, the macrophages as live vectors have been studied in *in vivo* models for several years. Further, several research groups have investigated the surface modification of NPs as a technique to increase NPs uptake capacity of macrophages including coating NPs with phosphatidylserine, polyethylene glycol, clathrin, and caveolin [28–34]. However, these coating techniques could often be challenging due to NPs heterogeneity.

In the present study, we demonstrated activated macrophages M1 with LPS stimulation as an efficient alternative to increase NPs uptake capacity. First, one of the M1 characteristics is high phagocytic activity for M*Φ* [35,36]. Owing to this, M1 has a 20-fold increase in uptake capacity of NPs, we confirmed this by applying QPI technique which provides a high-resolution 3-D tomography of phase-based information that measures particles per volume as shown in Fig. 1(c) and Table 1. With the 20-fold increase, NPs density was lower, approximately 1.4 pM, as compared to a previous study [9], 27.5 pM. However, NPs' density of 1.4 pM could not achieve an adequate temperature of 44 °C within 5 min, therefore, 3.0 pM was chosen as the optimum density of NPs in the present study, indicating a 9-fold decrease from the previous study. Although there was a decrease in the NPs concentration, it led to enhanced heat efficiency with laser irradiation.

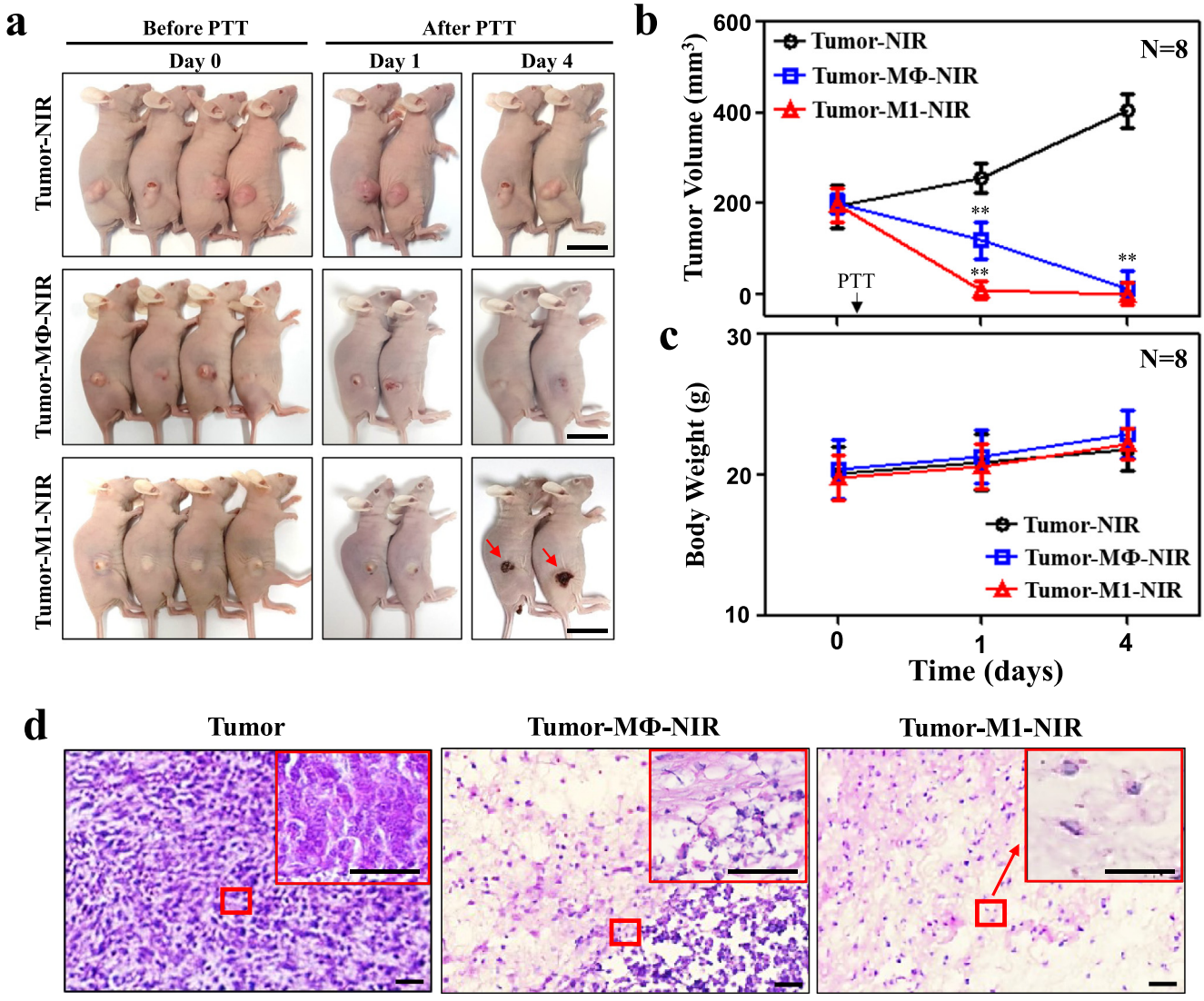

Fig. 4. The effect of PTT using NPs-loaded MΦ and M1. (a) The pictures of mice before and after PTT for 4 days. Red arrows indicate the indurated tissues with a crust caused by heat damage after PTT. Scale bar is 2 cm. (b) and (c) The reduction of tumor size and body weight were measured before and after PTT for 4 days. (d) The immunohistology (H&E) showed the image of a tissue section from the tumor site 12 h after PTT. Insets are the enlarged red boxes area in (d). Scale bar is 50 μm.

Second, another characteristic of M1 is fostering inflammatory response against invading pathogens and tumor cells, therefore M1 can easily infiltrate into the tumor microenvironment. On the other hand, while non-activated MΦ is a phagocytic scavenger cell and can recognize the signals released by cells undergoing necrosis, it has no direct specificity for cancer cells. Additionally, although MΦ responds to signals released by cancer cells such as hypoxic, apoptotic, and necrotic signals, it may not lead to active migration toward tumor mass.

In the present study, we conducted *in vivo* study which showed enhanced infiltration of peritumorally-injected M1 into the surrounding tumor mass, unlike in the previous study that used MΦ [10]. To evaluate the difference in migration capability between MΦ and M1, bioluminescence imaging with the luciferase gene transfected macrophages (MΦ and M1) was used. Although the bioluminescence imaging is not a quantitative assay and provides 2-D projection only, it offers a non-invasive, real-time analysis of longitudinal intact observation of the tumor mass inside. This bioluminescence imaging showed M1 with high luciferase expression intensity actively moved from four injection points to the tumor mass 12 h after injection, while MΦ seemed to have less active penetration with its intensity gradually diminishing in 72 h. The luciferase expression intensity of M1 in the center of tumor mass was 2.9-fold higher than that of MΦ at 12 h. Additionally, the tumor size reduction for MΦ and M1 groups in 4 days after PTT was 93.0% and 99.7%. However, the gap between these two groups was much larger in 1 day after PTT, 40.7% and 94.9% for MΦ and M1 group respectively, a 2.3-fold higher reduction in tumor size implying that the PTT efficiency was more apparent for M1. Overall, combining the effect of a 2-fold increase in NPs uptake capacity for and a 2.9-fold increase in penetrating capability for M1 over MΦ is likely to achieve an approximately 6-fold increase in PTT efficiency. We believe that M1 showing a 2.3-fold higher tumor mass size reduction could imply this 6-fold increase in PTT efficiency.

Furthermore, we administered PTT using a NIR laser with 1 W/cm^2 for 1 min in an animal model, the laser irradiation time was shorter than the previous study (1 W/cm^2 for 2 min) [10]. The M1 group showed more crust formations compared to the MΦ group in the irradiation region in 4 days after PTT, indicating that stronger photothermal energy was generated which caused more thermal damage to the surrounding tissues even with the shorter

irradiation time. Considering such risk, we may apply shorter irradiation time or lower power for M1 loaded NPs. Most of the crust formations healed 2 weeks after PTT, although not applied in this study, reducing either the NIR laser power or the irradiation time could be considered for minimizing the normal tissue damage.

Despite the supportive research findings, the incorporation of macrophages in cancer treatment is faced with some limitations. Activated macrophages are classified as M1 and M2 phenotypes [37–39]. M1 elicits inflammation response against invading pathogens and tumor cells, whereas M2 has immunoregulatory functions, angiogenesis, remodeling the tumor extracellular matrix to aid invasion, and tumor progression. However, recently, the classification of macrophage immune-activated states such as M1 and M2 is currently challenging because their functional phenotypes could lead to changes of the macrophage polarized activation states in the tumor microenvironment. It means that the repolarization between M1 and M2 could occur depending on the microenvironment they are embedded in [40,41]. The accumulation of M2 in the tumor microenvironment could lead to worse prognosis shown in previous clinical observations [42,43]. With iNOS immunohistochemical staining as a classical M1 marker, we confirmed M1 in the present study, a pro-inflammatory phenotype known to have anti-tumorigenic effects. Since the NPs-loaded M1 were destroyed by PTT at 12 h after injection, they would not be possible to play a role as M2 tumor-associated macrophages and lead to the accumulation of M2 in the tumor microenvironment.

Conclusion

In conclusion, the present study demonstrated an *in vivo* study that utilized the tumor-associated active migration feature of M1 macrophages. As a live vector, NPs-loaded M1 were injected peritumorally and actively infiltrated into the tumor mass in xenograft mice. In addition, M1 showed significant increases in the NPs uptake capacity and the penetrating capability into the tumor mass. Consequently, PTT with NPs-loaded M1 was more effective in tumor destruction compared to that with NPs-loaded MΦ. By utilizing this concept to make the improvement of PTT efficiency feasible, we believe PTT can be combined with other conventional methods to enhance tumor treatment for better overall prognosis.

Declaration of Competing Interest

The authors declare that they have no known competing financial interests or personal relationships that could have appeared to influence the work reported in this paper.

Acknowledgments

We thank Dr. Chang-Min Lee for helpful comments and discussions. This research was supported by the Clinical Trial Center of Korea University Anam Hospital (I1500931), the Korea Health Technology R&D Project (HI14C0748) through the Korea Health Industry Development Institute (KHIDI) by the Ministry of Health & Welfare, and the Basic Science Research Program through the National Research Foundation of Korea funded by the Ministry of Education (NRF-2016R1D1A1A02937362, NRF-2018R1D1A1A09083263, NRF-2019R1A2C4004804, and NRF-2019H1A2A1076334), and National Eye Institute (R01EY030569). Institute of Information and Communications Technology Planning and Evaluation (IITP; MSIT) (2020-0-00997). This research was also supported by a grant from Korea University.

Compliance with ethics requirements

All institutional and national guidelines for the care and use of animals (The Korea University Institutional Animal Care and Use Committee) were followed.

References

[1] Mann J. Natural products in cancer chemotherapy: past, present and future. Nat Rev Cancer 2002;2(2):143–8.
[2] Kaminski JM, Kaminski RJ, Dicker AP, Urbain JLC. Defining a future role for radiogenic therapy. Cancer Treat Rev 2001;27(5):289–94.
[3] Dunphy FR, Spitzer G, Fornoff JER, Yau JC, Huan SD, Dicke KA, et al. Factors predicting long-term survival for metastatic breast cancer patients treated with high-dose chemotherapy and bone marrow support. Cancer 1994;73 (8):2157–67.
[4] Cheng J-H, Chuang VP, Cheng SH, Huang AT, Lin Y-M, Cheng T-I, et al. Local radiotherapy with or without transcatheter arterial chemoembolization for patients with unresectable hepatocellular carcinoma. Int J Radiation Oncology Biol Phys 2000;47(2):435–42.
[5] Fang J, Chen YC. Nanomaterials for photohyperthermia: a review. Curr Pharm Des 2013;19(37):6622–34.
[6] Baek S-K, Makkouk AR, Krasieva T, Sun C-H, Madsen SJ, Hirschberg H. Photothermal treatment of glioma; an in vitro study of macrophage-mediated delivery of gold nanoshells. J Neurooncol 2011;104(2):439–48.
[7] Elsayed I, Huang X, Elsayed M. Selective laser photo-thermal therapy of epithelial carcinoma using anti-EGFR antibody conjugated gold nanoparticles. Cancer Lett 2006;239(1):129–35.
[8] Hirsch LR, Stafford RJ, Bankson JA, Sershen SR, Rivera B, Price RE, et al. Nanoshell-mediated near-infrared thermal therapy of tumors under magnetic resonance guidance. Proc Natl Acad Sci USA 2003;100(23):13549–54.
[9] Yang TD, Choi W, Yoon TH, Lee KJ, Lee J-S, Han SH, et al. Real-time phase-contrast imaging of photothermal treatment of head and neck squamous cell carcinoma: an in vitro study of macrophages as a vector for the delivery of gold nanoshells. J Biomed Opt 2012;17(12):128003. doi: https://doi.org/10.1117/1.JBO.17.12.12800310.1117/1.JBO.17.12.128003.2.
[10] Yang TD, Choi W, Yoon TH, Lee KJ, Lee J-S, Joo JH, et al. In vivo photothermal treatment by the peritumoral injection of macrophages loaded with gold nanoshells. Biomed Opt Express 2016;7(1):185. doi: https://doi.org/10.1364/BOE.7.00018510.1364/BOE.7.000185.v001.
[11] Yang TD, Park K, Kim H-J, Im N-R, Kim B, Kim T, et al. In vivo photothermal treatment with real-time monitoring by optical fiber-needle array. Biomed Opt Express 2017;8(7):3482. doi: https://doi.org/10.1364/BOE.8.00348210.1364/BOE.8.003482.v00110.1364/BOE.8.003482.v002.
[12] Tarique AA, Logan J, Thomas E, Holt PG, Sly PD, Fantino E. Phenotypic, functional, and plasticity features of classical and alternatively activated human macrophages. Am J Respir Cell Mol Biol 2015;53(5):676–88.
[13] Normanno N, De Luca A, Bianco C, Strizzi L, Mancino M, Maiello MR, et al. Epidermal growth factor receptor (EGFR) signaling in cancer. Gene 2006;366 (1):2–16.
[14] Dickerson EB, Dreaden EC, Huang X, El-Sayed IH, Chu H, Pushpanketh S, et al. Gold nanorod assisted near-infrared plasmonic photothermal therapy (PPTT) of squamous cell carcinoma in mice. Cancer Lett 2008;269(1):57–66.
[15] Barua S, Mitragotri S. Challenges associated with penetration of nanoparticles across cell and tissue barriers: A review of current status and future prospects. Nano Today 2014;9(2):223–43.
[16] Christie C, Madsen SJ, Peng Q, Hirschberg H. Photothermal therapy employing gold nanoparticle- loaded macrophages as delivery vehicles: comparing the efficiency of nanoshells versus nanorods. J Environ Pathol Toxicol Oncol 2017;36(3):229–35.
[17] Mills C. M1 and M2 macrophages: oracles of health and disease. Crit Rev Immunol 2012;32(6):463–88.
[18] Ley K. M1 means kill; M2 means heal. J Immunol 2017;199(7):2191–3.
[19] Yuan A, Hsiao Y-J, Chen H-Y, Chen H-W, Ho C-C, Chen Y-Y, et al. Opposite effects of M1 and M2 macrophage subtypes on lung cancer progression. Sci Rep 2015;5(1). doi: https://doi.org/10.1038/srep14273.
[20] Miao X, Leng X, Zhang Q. The current state of nanoparticle-induced macrophage polarization and reprogramming research. Int J Mol Sci 2017;18 (2).
[21] Qie Y, Yuan H, von Roemeling CA, Chen Y, Liu X, Shih KD, et al. Surface modification of nanoparticles enables selective evasion of phagocytic clearance by distinct macrophage phenotypes. Sci Rep 2016;6(1). doi: https://doi.org/10.1038/srep26269.
[22] Stöber W, Fink A, Bohn E. Controlled growth of monodisperse silica spheres in the micron size range. J Colloid Interface Sci 1968;26(1):62–9.
[23] Choi Y, Kim M, Yoon C, Yang TD, Lee KJ, Choi W. Synthetic aperture microscopy for high resolution imaging through a turbid medium. Opt Lett 2011;36 (21):4263. doi: https://doi.org/10.1364/OL.36.00426310.1364/OL.36.004263.m00110.1364/OL.36.004263.m002.
[24] Kasprowicz R, Suman R, O'Toole P. Characterising live cell behaviour: Traditional label-free and quantitative phase imaging approaches. Int J Biochem Cell Biol 2017;84:89–95.

[25] McWhorter FY, Wang T, Nguyen P, Chung T, Liu WF. Modulation of macrophage phenotype by cell shape. Proc Natl Acad Sci USA 2013;110 (43):17253–8.
[26] Heinrich F, Lehmbecker A, Raddatz BB, Kegler K, Tipold A, Stein VM, et al. Morphologic, phenotypic, and transcriptomic characterization of classically and alternatively activated canine blood-derived macrophages in vitro. PLoS One. 2017;12(8):e0183572.
[27] Yang TD, Park K, Park JS, Lee JH, Choi E, Lee J, et al. Two distinct actin waves correlated with turns-and-runs of crawling microglia. PLoS One. 2019;14(8): e0220810.
[28] Fang RH, Kroll AV, Gao W, Zhang L. Cell membrane coating nanotechnology. Adv Mater 2018;30(23):1706759. doi: https://doi.org/10.1002/adma.v30.2310.1002/adma.201706759.
[29] Shi J, Kantoff PW, Wooster R, Farokhzad OC. Cancer nanomedicine: progress, challenges and opportunities. Nat Rev Cancer 2017;17(1):20–37.
[30] Barrera C, Herrera AP, Rinaldi C. Colloidal dispersions of monodisperse magnetite nanoparticles modified with poly(ethylene glycol). J Colloid Interface Sci 2009;329(1):107–13.
[31] Tempone AG, Perez D, Rath S, Vilarinho AL, Mortara RA, de Andrade HF, et al. Targeting Leishmania (L.) chagasi amastigotes through macrophage scavenger receptors: the use of drugs entrapped in liposomes containing phosphatidylserine. J Antimicrob Chemother 2004;54(1):60–8.
[32] Cattel L, Ceruti M, Dosio F. From conventional to stealth liposomes: a new frontier in cancer chemotherapy. J Chemother 2004;16(sup4):94–7.
[33] Singh S, Kumar A, Karakoti A, Seal S, Self WT. Unveiling the mechanism of uptake and sub-cellular distribution of cerium oxide nanoparticles. Mol BioSyst 2010;6(10):1813. doi: https://doi.org/10.1039/c0mb00014k.
[34] Hill MM, Bastiani M, Luetterforst R, Kirkham M, Kirkham A, Nixon SJ, et al. PTRF-cavin, a conserved cytoplasmic protein required for caveola formation and function. Cell 2008;132(1):113–24.
[35] Orecchioni M, Ghosheh Y, Pramod AB, Ley K. Macrophage polarization: different gene signatures in M1(LPS+) vs. classically and M2(LPS-) vs. alternatively activated macrophages. Front Immunol. 2019;10:1084.
[36] Cheng H, Wang Z, Fu L, Xu T. Macrophage polarization in the development and progression of ovarian cancers: an overview. Front Oncol 2019;9:421.
[37] Biswas SK, Mantovani A. Macrophage plasticity and interaction with lymphocyte subsets: cancer as a paradigm. Nat Immunol 2010;11(10):889–96.
[38] Bertani FR, Mozetic P, Fioramonti M, Iuliani M, Ribelli G, Pantano F, et al. Classification of M1/M2-polarized human macrophages by label-free hyperspectral reflectance confocal microscopy and multivariate analysis. Sci Rep 2017;7(1). doi: https://doi.org/10.1038/s41598-017-08121-8.
[39] Pajarinen J, Tamaki Y, Antonios JK, Lin T-H, Sato T, Yao Z, et al. Modulation of mouse macrophage polarization in vitro using IL-4 delivery by osmotic pumps : Modulation of macrophage polarization by IL-4 delivery. J Biomed Mater Res 2015;103(4):1339–45.
[40] Mantovani A, Sozzani S, Locati M, Allavena P, Sica A. Macrophage polarization: tumor-associated macrophages as a paradigm for polarized M2 mononuclear phagocytes. Trends Immunol 2002;23(11):549–55.
[41] Martinez FO, Gordon S. The M1 and M2 paradigm of macrophage activation: time for reassessment. F1000Prime Rep 2014. 6:13.
[42] Pollard JW. Macrophages define the invasive microenvironment in breast cancer. J Leukoc Biol 2008;84(3):623–30.
[43] Ohtaki Y, Ishii G, Nagai K, Ashimine S, Kuwata T, Hishida T, et al. Stromal macrophage expressing CD204 is associated with tumor aggressiveness in lung adenocarcinoma. J Thoracic Oncol 2010;5(10):1507–15.